Revista Mexicana de Astronomía y Astrofísica, **53**, 1–8 (2017)

AN APPROXIMATE ANALYTIC SOLUTION AND STABILITY CRITERION FOR THE LOGATROPIC SPHERE

S. Lizano[1], A. C. Raga[2], and J. C. Rodríguez-Ramírez[2]

Received December 5 2016; accepted June 30 2017

ABSTRACT

A logatropic equation of state (in which the pressure is proportional to the logarithm of the gas density) has been used in models of molecular clouds to mimic turbulent pressure. We explore solutions of the associated logatropic Lane-Emden equation, describing the hydrostatic equilibrium of a self-gravitating sphere with a logatropic equation of state. We present approximate analytic solutions for the small radius behavior of the non-singular solution, and for its large radius convergence to the singular solution. Combining a "small radius" and a "large radius" solution, we obtain an analytic approximation to the full, non-singular solution. Using both an exact (numerical) and the approximate analytic solution, we apply Bonnor's stability criterion, and determine the stability of the non-singular solution of the logatropic, self-gravitating sphere.

RESUMEN

Una ecuación de estado logatrópica (en la que la presión es proporcional al logaritmo de la densidad del gas) ha sido empleada en modelos de nubes moleculares para imitar una presión turbulenta. Exploramos soluciones a la correspondiente ecuación de Lane-Emden logatrópica, que describe el equilibrio hidrostático de una esfera autogravitante con una ecuación de estado logatrópica. Presentamos soluciones analíticas aproximadas para el comportamiento a radios pequeños de la solución no singular, y para su convergencia a radios grandes a la solución singular. Combinando soluciones para "radios pequeños" y para "radios grandes", obtenemos una aproximación analítica completa para la solución no singular. Usando la solución exacta (numérica) y la solución analítica aproximada, aplicamos el criterio de estabilidad de Bonnor, y determinamos la estabilidad de la solución no singular de una esfera logatrópica autogravitante.

Key Words: equation of state — ISM: clouds — stars: formation

1. INTRODUCTION

The logatropic equation of state was first proposed by Lizano & Shu (1989) motivated by the empirical finding in molecular clouds that the non-thermal part of the line widths in molecular gas tracers increases with decreasing densities, so that $\Delta v \propto \rho^{-1/2}$ in low mass cores (e.g., Fuller & Myers 1992). The interpretation of these line widths as due to an isotropic velocity dispersion $\sigma^2 = dP/d\rho$ (where P is the pressure and ρ is the density), gives the logatropic equation of state:

$$P = P_0 \ln\left(\frac{\rho}{\rho_0}\right), \quad \text{with} \quad \sigma^2 = \frac{P_0}{\rho}, \qquad (1)$$

where P_0 and ρ_0 are a reference pressure and density, respectively[3].

Lizano & Shu (1989) used this equation of state to mimic the effect of turbulence in low mass cores, cradles of low mass stars. McLaughlin and Pudritz (1996; 1997) analyzed the stability and collapse of self-gravitating gas spheres with a logatropic pressure. The hydrostatic gas equation has a singular

[1]Instituto de Radioastronomía y Astrofísica, UNAM, México.

[2]Instituto de Ciencias Nucleares, UNAM, México.

[3]The reference density can be chosen so that $P > 0$; nevertheless, the equilibrium and collapse equations of a self-gravitating sphere contain only the pressure gradient $dP/d\rho$.

solution with a radial density profile $\rho \propto r^{-1}$. Because the free-fall time is shortest in the center, the gravitational collapse occurs inside-out: an expansion wave moves outward and the inner gas falls to the central protostar, as in the case of the singular isothermal sphere (Shu 1977). The mass accretion rate grows with time as $\dot{M} \propto t^3$, in contrast with the isothermal sphere where $\dot{M}$ grows linearly with time. The collapse of non-singular, finite, logatropic spheres was studied numerically by Reid et al. (2002) and Sigalotti et al. (2002). Osorio et al. (1999) and Osorio et al. (2009) modeled hot molecular cores (HMCs) around young massive stars as massive logatropic envelopes collapsing onto a central protostar. The fitting of the spectral energy distribution (SED) and molecular line emission implied large mass accretion rates $\dot{M} \approx 10^{-4} - 10^{-3} M_\odot\,\mathrm{yr}^{-1}$ and ages $\tau_{\rm age} \approx 4 - 6 \times 10^4\,\mathrm{yr}$, and the accretion luminosity dominates the core heating. Sigalotti et al. (2009) followed the gravitational collapse of pressure-bounded logatropic HMCs and found that the collapse is not reversed by radiative forces on the dust; stars as massive as $100 M_\odot$ can form by accretion of these massive envelopes.

Observations of the radial intensity profiles of massive star forming regions imply envelopes with a density distribution $\rho \propto r^{-p}$ with indices $1 < p < 2$, with uncertainties due to issues like the temperature distribution, optical depth, and geometrical effects (e.g., Hatchell et al. 2000; van der Tak et al. 2000; Beuther et al. 2002; Hatchell et al. 2003). These density profiles are expected for isothermal and logatropic self-gravitating spheres. An interesting problem is whether or not these density distributions could be established in the process of accretion via gas streams onto massive star forming cores (e.g., Peretto et al. (2013); Liu et al. (2015)).

Following Raga et al. (2013a; hereafter R2013a) in this paper we derive a new analytic approximation for the density and mass of a non-singular, logatropic, self-gravitating gas sphere. This solution differs by less than 0.2% from the exact (numerical) solution. We then use the criterion of Bonnor (1956) to obtain analytically and numerically the gravitational stability of finite logatropic spheres to radial perturbations (as done by Raga et al. 2013b for the case of the isothermal sphere) and find the maximum radius of a stable logatropic sphere.

The paper is organized as follows: in §2 we discuss the Lane-Emden equation and the singular solution. In §3 we discuss the non-dimensional equations and obtain the second order inner solution. In §4 we discuss the convergence to the singular solution at large radii. In §5 we present the full analytic solution for the dimensionless density and mass. In §6 we calculate the criterion of gravitational stability to radial perturbations and find the maximum radius of a gravitationally stable logatropic gas sphere. Finally, in §7 we present the conclusions.

2. HYDROSTATIC SELF-GRAVITATING LOGATROPIC SPHERE

The hydrostatic equation for a self-gravitating gas sphere is:

$$\frac{dP}{dR} = -\frac{\rho G M_R}{R^2}\,, \tag{2}$$

where R is the spherical radius, G the gravitational constant and the mass within a radius R is:

$$M_R = 4\pi \int_0^R \rho R'^2 dR'. \tag{3}$$

Combining equations (2) and (3) with the logatropic equation of state in Equation (1), multiplying both sides of the resulting equation by R^2/ρ and taking a d/dR derivative we obtain the logatropic Lane-Emden equation:

$$\frac{d}{dR}\left(\frac{R^2}{\rho^2}\frac{d\rho}{dR}\right) = -\frac{4\pi G}{P_0}\rho R^2\,. \tag{4}$$

This equation has the singular solution:

$$\rho_S(R) = \sqrt{\frac{P_0}{2\pi G}}\frac{1}{R}\,. \tag{5}$$

3. THE NON-SINGULAR SOLUTION TO SECOND ORDER IN R AND THE DIMENSIONLESS EQUATION

To derive a "small R" behavior of the non-singular solution of the Lane-Emden Equation (4), we propose a second-order Taylor series expansion:

$$\rho_2(R) = \rho_c\left(1 + b_1 R + b_2 R^2\right) \tag{6}$$

where ρ_c is the central density and b_1 and b_2 are constants to be determined. We then substitute eq. (6) in the two sides of eq. (4), and keep only terms up to second order in R. Equating the coefficients that multiply the R and R^2 terms we obtain $b_1 = 0$ and

$$b_2 = -\frac{1}{R_c^2}\,, \tag{7}$$

where the core radius R_c is defined as:

$$R_c \equiv \sqrt{\frac{3P_0}{2\pi G \rho_c^2}}\,. \tag{8}$$

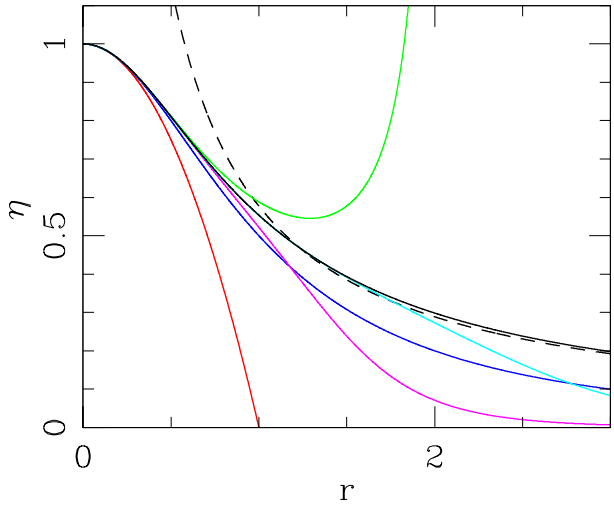

Fig. 1. Dimensionless density vs. dimensionless radius for the exact (numerical) non-singular solution (black, solid line), the second order non-singular solution (red, solid line) and the singular solution (dashed line). The alternative second order solution (blue line), the 4th order solution (green), the 6th order solution (magenta) and the "near field" fit (cyan) described in § 4.1 are also shown. The color figure can be viewed online.

Therefore, the second order solution can be written as:

$$\rho_2(R) = \rho_c \left[1 - \left(\frac{R}{R_c}\right)^2\right] . \tag{9}$$

With the dimensionless density $\eta = \rho/\rho_c$ and dimensionless radius $r = R/R_c$, equation (4) now takes the form:

$$\frac{d}{dr}\left(\frac{r^2}{\eta^2}\frac{d\eta}{dr}\right) = -6r^2\eta\,. \tag{10}$$

This dimensionless logatropic Lane-Emden equation can be integrated numerically in a straightforward fashion. Starting at an initial radius $r_i \ll 1$, so that the second order solution:

$$\eta_2(r) = 1 - r^2\,, \tag{11}$$

is valid (see equation 9), one can integrate outwards to large r. The black solid line in Figure 1 shows the numerical $\eta(r)$ solution, where one can see the convergence for $r \gg 1$ to the singular solution:

$$\eta_S(r) = \frac{1}{\sqrt{3}r}\,, \tag{12}$$

as a dashed line (see Equation 5). The second-order solution inner solution (Equation 11), valid for $r \ll 1$, is shown as a red line.

4. THE LARGE R CONVERGENCE TO THE SINGULAR SOLUTION

As has been done in the past for the non-singular isothermal sphere solution (see, e.g., Chandrasekhar 1964; R2013a), we now study the large r convergence of the non-singular logatropic sphere to the singular solution. In order to do this, we define a function $q(r)$ such that:

$$\eta(r) = \eta_S(r)\,[1 + q(r)]\,, \tag{13}$$

where $\eta(r)$ is the non-singular solution of equation (10) and $\eta_S(r)$ is the singular solution (equation 12).

We substitute equation (13) in both sides of equation (10), and assuming that q, dq/dr, $d^2q/dr^2 \ll 1$, we only keep the terms that depend linearly on q and its derivatives. This exercise results in the differential equation:

$$r^2\frac{d^2q}{dr^2} + 4r\frac{dq}{dr} + 4q = 0\,. \tag{14}$$

Assuming a solution of the form $q \propto r^p$ and substituting into equation (14) one obtains an exponent $p = (-3 \pm \sqrt{7}i)/2$. Then, the real part of the solution is:

$$q_l(r) = \frac{B}{r^{3/2}}\cos\left(\frac{\sqrt{7}}{2}\ln r + \phi\right)\,, \tag{15}$$

where B and ϕ are integration constants. This oscillating solution at large radii has the same period (in $\ln r$) as the one found for the isothermal sphere (see equation 15 of R2013a). Nevertheless, the amplitude decreases much faster with radius, like $r^{-3/2}$, rather than the slower $r^{-1/2}$ dependence obtained for the isothermal sphere.

5. AN APPROXIMATE ANALYTIC SOLUTION

In this section we present an analytic approximation for the density $\eta(r)$ over the whole $0 < r < \infty$ interval.

5.1. *The "Near Field" Solution*

For the small r regime, one can in principle use the second order Taylor series solution (see equation 11), but this solution starts diverging from the exact (i.e., numerical) solution for r substantially smaller than 1 (see Figure 1). An alternative second order solution is:

$$\eta_{2p}(r) = \frac{1}{1 + r^2}\,, \tag{16}$$

which to second order coincides with equation (11). As seen Figure 1, this solution (plotted as a blue line) is a better approximation to the exact solution.

One can look for functions in the form of the inverse of a polynomial (such as equation 16), that are solutions to higher orders in r of the logatropic hydrostatic equation (10). To 4th order one obtains:

$$\eta_{4p}(r) = \frac{1}{1 + r^2 - (3/10)r^4}\,, \tag{17}$$

and to 6th order one obtains:

$$\eta_{6p}(r) = \frac{1}{1 + r^2 - (3/10)r^4 + (13/60)r^6}\,. \tag{18}$$

From Figure 1, we see that η_{2p} substantially undershoots (blue line), η_{4p} overshoots (green line) and η_{6p} again undershoots (magenta line) the exact solution. This lack of convergence for $r \to 1$ (obtained for arbitrarily high orders of r) is also seen in the isothermal Lane-Emden equation (see, e.g., Nouh 2004).

An approximate fitting formula can be obtained by considering the 4th order solution of equation (17) and adding a 5th order term to the polynomial, with an arbitrary coefficient that is used to fit the exact (numerical) solution. In this way, we obtain a "near field" solution (with a "fitting" fifth order term, not coming from a Taylor series expansion) of the form:

$$\eta_{near}(r) = \frac{1}{1 + r^2 - (3/10)r^4 + 0.1082r^5}\,. \tag{19}$$

The errors in this approximate form for the small r regime of $\eta(r)$ are discussed in § 5.3.

5.2. *The "Far Field" Solution*

For large values of r, we use the analytic solution of § 4 (see Equations 13 and 15), obtaining the B and ϕ constants from a fit to the exact (numerical) solution. In this way, we obtain a "far field" solution of the form:

$$\eta_{far}(r) = \frac{1 + q_{far}(r)}{\sqrt{3}r}\,, \tag{20}$$

with

$$q_{far}(r) = -\frac{0.155}{r^{3/2}}\cos\left(\frac{\sqrt{7}}{2}\ln r + 1.295\right)\,. \tag{21}$$

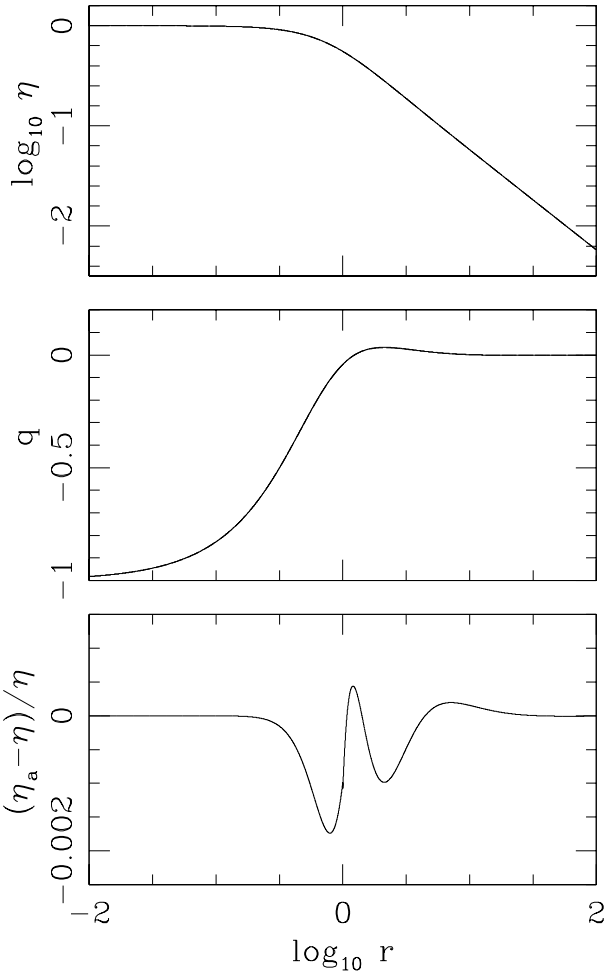

Fig. 2. Top: density vs. radius for the exact (numerical) non-singular solution (solid line). Center: deviation $q = \eta/\eta_S - 1$ (see equation 13) of the exact solution from the singular solution. Bottom: deviation $\eta_a/\eta - 1$ between the full near/far field analytic approximation (equation 22) and the exact numerical solution. In the two top frames we have also plotted the results obtained using η_a (instead of the exact solution, as dashed lines), but at the resolution of the plots they are indistinguishable from the solid curves corresponding to the exact solution.

5.3. *The Full Approximate Analytic Solution*

We propose an approximate analytic solution for all r given by:

$$\eta_a(r) = \begin{cases} \eta_{near}(r)\,; & \text{for } r \le 1, \\ \eta_{far}(r)\,; & \text{for } r > 1. \end{cases} \tag{22}$$

The top panel of Figure 2 shows the logarithm of the dimensionless density η versus the logarithm of radius r for the exact (numerical) solution and the

approximate near/far field solution of equation (22). Both solutions are indistinguishable at the resolution of the figure. The middle panel shows the difference between the exact (numerical) non-singular solution and the singular solution, $q = \eta/\eta_S - 1$, as a function of r (see equation 13). Again, the results obtained with the exact and approximate analytic solutions are indistinguishable. Only the first oscillation of the far-field solution appears because the rest are attenuated by the factor $r^{-3/2}$ (see Figure 4 below). The relative deviation $(\eta_a - \eta)/\eta$ of the analytic approximation η_a from the exact (numerical) non-singular solution is plotted as a function of r in the bottom panel of Figure 2. It is clear that the errors in η_a are smaller than $\approx 0.2\%$ for all r. Because of this, at the resolution of the top panels of this figure, the analytic approximation is indistinguishable from the exact (numerical) solution.

5.4. *Mass as a Function of Radius of the Non-Singular Logatropic Sphere*

The mass of the non-singular logatropic sphere within a radius R is:

$$M(R) = 4\pi\rho_c R_c^3\, m(r)\,, \tag{23}$$

where ρ_c and R_c are related through equation (8) and the dimensionless mass is given by:

$$m(r) = \int_0^r \eta(r') r'^2 dr'\,. \tag{24}$$

The dimensionless mass can also be obtained from the dimensionless form of Equation (2):

$$m(r) = -\frac{1}{6}\frac{r^2}{\eta^2}\frac{d\eta}{dr}, \tag{25}$$

which is easy to calculate using the analytic dimensionless density, $\eta_a(r)$. The upper panel of Figure 3 shows the exact (numerical) mass $m(r)$ and the dotted line shows the analytic mass $m_a(r)$ which are indistinguishable at the resolution of the plot. The lower panel shows the fractional difference between the analytic and exact (numerical) mass, $(m_a - m)/m$. This difference is smaller than 2%.

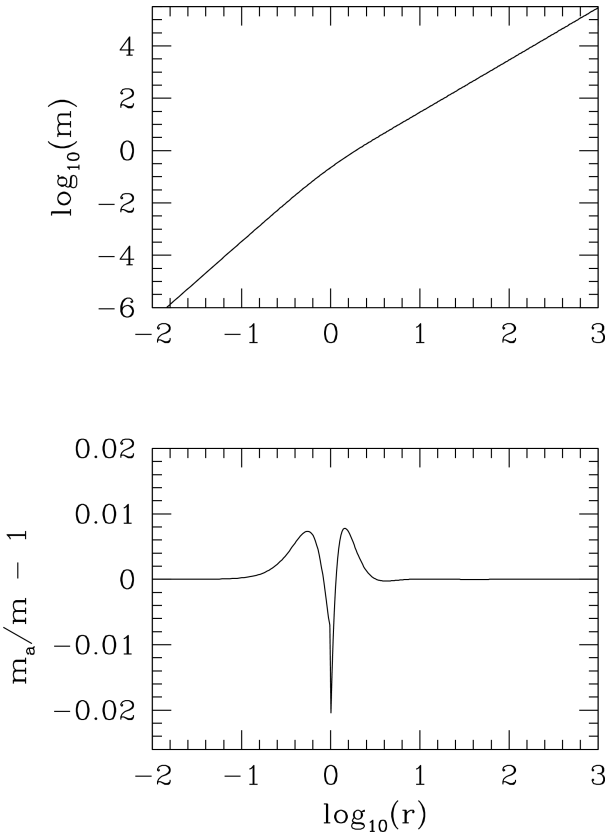

Fig. 3. The solid line in the upper panel shows the exact (numerical) mass $m(r)$ and the dotted line shows the analytic mass $m_a(r)$ obtained from equation 25. The lower panel shows the fractional difference between the analytic and exact (numerical) masses, $(m_a - m)/m$, where the modulus is always smaller than 0.02.

6. STABILITY TO RADIAL PERTURBATIONS

The radial stability analysis of the isothermal self-gravitating finite gas sphere was done by Bonnor (1956) and Ebert(1957) who showed that there is a maximum radius for an isothermal sphere to be stable to gravitational collapse. Bonnor (1956) proposed the criterion for stability of a finite isothermal self-gravitating gas sphere with radius R_e and total mas M against radial perturbations,

$$\left(\frac{dP_e}{dR_e}\right)_{M=const} < 0. \tag{26}$$

In the case of a logatropic sphere, this criterion becomes:

$$\frac{P_0}{\rho_e}\left(\frac{d\rho_e}{dR_e}\right)_{M=const} < 0, \tag{27}$$

where $\rho_e = \rho(R_e)$. McLaughlin and Pudritz (1996) calculated the stability of the logatropic sphere assuming that the singular solution was valid at the external radius r_e (see their equation 4.6). Here we calculate this criterion from the exact (numerical) and analytic solutions (the latter given by equation 22) following Raga et al. (2013b), who calculated the stability of an isothermal gas sphere to radial perturbations.

In dimensional units one can write the logatropic density at the external radius R_e as:

$$\rho_e = \rho_c \eta_e = \frac{C}{R_c}\eta(r_e), \quad \text{where} \quad C = \sqrt{\frac{3P_0}{2\pi G}}, \quad (28)$$

and the dimensional mass inside a radius R_e as:

$$M(R_e) = 4\pi C R_c^2 m(r_e), \quad (29)$$

where $r_e = R_e/R_c$, $m(r)$ is given by Equation (24), and we have used Equation (8) for the core radius R_c.

One wants to consider radial perturbations of a sphere at constant mass. First, one differentiates Equation (29), obtaining:

$$\frac{dM}{4\pi C} = 2mR_c dR_c + R_c^2 m' \left[\frac{\partial r_e}{\partial R_c} dR_c + \frac{\partial r_e}{\partial R_e} dR_e\right] \quad (30)$$

$$= R_c \left[2m + R_c m' \frac{\partial r_e}{\partial R_c}\right] dR_c + R_c^2 m' \frac{\partial r_e}{\partial R_e} dR_e, \quad (31)$$

where, from equation (24),

$$m' \equiv \frac{dm(r_e)}{dr_e} = r_e^2 \eta_e. \quad (32)$$

Setting $dM = 0$ and substituting $\partial r_e/\partial R_c = -r_e/R_c$, $\partial r_e/\partial R_e = 1/R_c$, one obtains:

$$0 = R_c \left[2m - r_e m'\right] dR_c + R_c m' dR_e. \quad (33)$$

Therefore, for radial variations at constant mass, one can write the derivative of the core radius with respect to the external boundary as:

$$\frac{dR_c}{dR_e} = \frac{m'}{r_e m' - 2m} = \frac{1}{r_e - 2m/m'}. \quad (34)$$

The criterion for stability is $d\rho_e/dR_e > 0$ (see equation 27). In the logatropic sphere, this derivative is:

$$\frac{1}{C}\frac{d\rho_e}{dR_e} = -\eta \frac{1}{R_c^2}\frac{dR_c}{dR_e} + \frac{1}{R_c}\frac{d\eta}{dr_e}\frac{dr_e}{dR_e} \quad (35)$$

$$= \frac{1}{R_c^2}\left(\frac{r_e^2\eta^2 + 2m\eta'}{2m - r_e^3\eta}\right), \quad (36)$$

where we have used equation (34) and

$$\frac{dr_e}{dR_e} = \frac{1}{R_c} - \frac{r_e}{R_c}\frac{dR_c}{dR_e}. \quad (37)$$

Substituting $m(r)$ in equation (25), the criterion for stability of the logatropic sphere against radial perturbations is:

$$\frac{R_c^2}{C}\frac{d\rho_e}{dR_e} = \frac{\frac{1}{3}\eta'^2 - \eta^4}{r_e\eta^3 + \frac{1}{3}\eta'} < 0. \quad (38)$$

The logarithm of the absolute value of this derivative is shown in Figure 4 where the solid line is obtained with the exact (numerical) solution $\eta(r)$ and the dotted-dashed line is obtained with the analytic solution $\eta_a(r)$ of equation (22). Both lines almost coincide. The arrow shows the dimensionless critical radius for stability:

$$r_{\rm crit} = 3.049, \quad (39)$$

where the derivative becomes negative. This is the maximum external radius for which one has a gravitationally stable configuration. In the notation of McLaughlin & Pudritz (1996), $r_{\rm crit}$ corresponds to $\xi_{\rm crit} = R_{\rm crit}/r_0 = (2A/3)^{1/2}3.049$, where A is their pressure parameter defined in their equation (4.1), and $r_0 = (3/2A)^{1/2}R_c$ is their scale radius. Our value of the critical radius (or $\xi_{\rm crit}$) differs from the value they obtained in their equation (4.6), $\xi_{\rm crit}^{MP} = (2A/9)^{1/2}\exp(1/A - 1/4)$. This difference is due to their use of the singular solution (η_S) to evaluate the stability criterion, and their constraint of a constant velocity dispersion at the center of the sphere. In contrast, we used the exact numerical solution (η) to evaluate the stability criterion, and we kept an invariant P vs. ρ relation (see equation 1), leading to a "heating" of the turbulent motions in the center of the cloud in response to small compressions.

There are other bands of stability with $r_e > r_{\rm crit}$ where the derivative is positive. These bands are related to the oscillations of $\eta(r)$ at large radii In order to visualize the oscillations of $\eta(r)$ at large radii, the dotted line in Figure 4 shows $r^{3/2}q(r)$, where $q = \eta/\eta_S - 1$ is the fractional deviation of the dimensionless density with respect to the singular solution of equation (12). Even though one could have a sphere with a larger radius $r_e > r_{\rm crit}$ where the derivative is positive, Bonnor (1956) argued that any radial perturbation would eventually reach an unstable inner region, inducing the overall collapse.

Given the critical radius $r_{\rm crit}$, the ratio between the central density ρ_c and the density at the cloud edge in a gravitationally stable logatropic sphere is given by:

$$\frac{\rho_c}{\rho(r_{\rm crit})} = \frac{1}{\eta(r_{\rm crit})} = \frac{1}{0.192} = 5.2, \quad (40)$$

which is smaller than the value of 14.7 obtained for the case of the isothermal sphere. Furthermore, the ratio of the velocity dispersions at the cloud center and at the cloud edge is $\sigma_c/\sigma(r_{\rm crit}) = \rho(r_{\rm crit})/\rho_c = 0.192$. Also, the Jeans

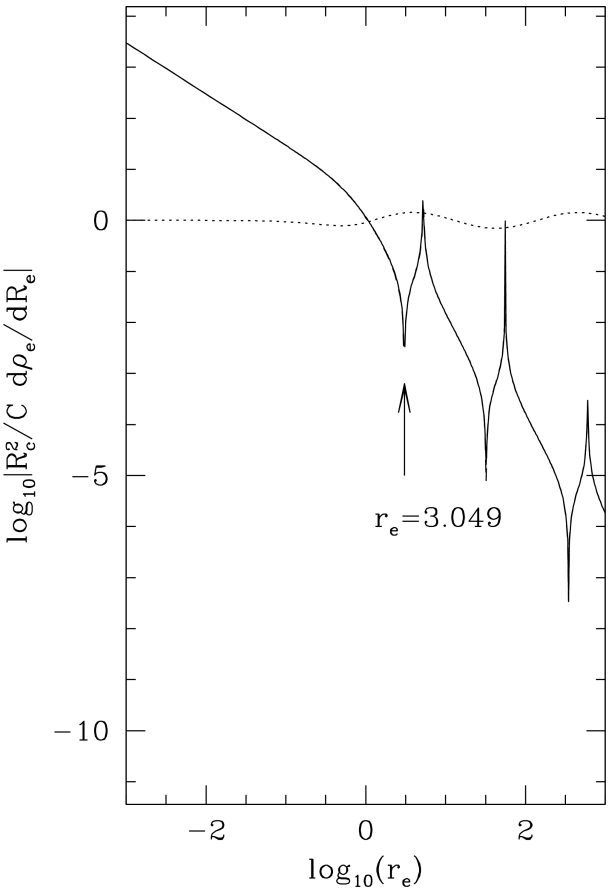

Fig. 4. The solid line shows the logarithm of the absolute value of the stability criterion in equation (38) obtained with the exact (numerical) solution $\eta(r)$, and the dotted-dashed line shows the derivative calculated with the analytic solution $\eta_a(r)$. Note that the cusps extend to $\pm\infty$ when the argument of the logarithm goes through zero. The dotted line shows $r^{3/2}q$, where $q = \eta/\eta_S - 1$ is the fractional deviation of the dimensionless density with respect to the singular solution.

length at the cloud center is $\lambda_J = c_s\sqrt{\pi/(G\rho_c)}$, where the sound speed is $c_s = \sigma = \sqrt{P_0/\rho_c}$. If we define the Jeans radius as $R_J = \lambda_J/2$, then the ratio of the cloud critical radius to the Jeans radius is $R_{\rm crit}/R_J = 2(3.049/\pi)(3/2)^{1/2} = 2.38$.

7. CONCLUSIONS

We present an approximate analytic solution for the density of the non-singular self-gravitating logatropic gas sphere that differs by less than 0.2% from the exact (numerical) solution. The analytic mass differs by less than 2% from the exact mass. This analytic function η_a (eq. (22) can be useful for the study of this type of clouds.

We calculate the gravitational stability of the logatropic sphere to radial perturbations and find a maximum external radius $R_{\rm crit} = 3.049\,R_c$, where the core radius is expressed in terms of the properties of the logatropic sphere $R_c = \sqrt{3P_0/(2\pi G\rho_c^2)}$. This value implies a maximum density ratio of the density at the cloud center to the density at the external radius, $\rho_c/\rho(r_{\rm crit}) = 5.2$, smaller than the factor of 14.7 which is obtained for the isothermal sphere.

SL acknowledges support from grants DGAPA-UNAM IN105815 and CONACytT 238631. AR acknowledges support from the CONACyT grants 167611 and 167625 and the DGAPA-UNAM grants IN109715, IG100516, IA103115 and IA103315.

REFERENCES

Beuther, H., Schilke, P., Menten, K. M., et al. 2002, ApJ, 566, 945
Chandrasekhar, S. 1967, An introduction to the study of stellar structure (Dover Publications: New York)
Bonnor, W. B. 1956, MNRAS, 116, 351
Ebert, R. 1957, Zeit. Atrophys., 42, 263
Fuller, G. A., & Myers, P. C. 1992, ApJ, 384, 523
Hatchell, J., Fuller, G. A., Millar, T. J., Thompson, M. A., & Macdonald, G. H. 2000, A&A, 357, 637
Hatchell, J. & van der Tak, F. F. S. 2003, A&A, 409, 589
Lizano, S. & Shu, F. H. 1989, ApJ, 342, 834
Liu, H. B., Galván-Madrid, R., Jiménez-Serra, I., et al. 2015, ApJ, 804, 37
Nouh, M. I. 2004, New. Astron., 9, 467
McLaughlin, D. E., & Pudritz, R. E. 1996, ApJ, 469, 194
_____. 1997, ApJ, 476, 750
Osorio, M., Lizano, S., & D'Alessio, P. 1999, ApJ, 525, 808
Osorio, M., Anglada, G., Lizano, S., & D'Alessio, P. 2009, ApJ, 694, 29
Peretto, N., Fuller, G. A., Duarte-Cabral, A., et al. 2013, A&A, 555, A112
Raga, A. C., Rodríguez-Ramírez, J. C., Villasante, M., Rodríguez-González, A., & Lora, V. 2013a, RMxAA, 49, 63
Raga, A. C., Rodríguez-Ramírez, J. C., Rodríguez-González, A., Lora, V., & Esquivel, A. 2013b, RMxAA, 49, 127
Reid, M. A., Pudritz, R. E., & Wadsley, J. 2002, ApJ, 570, 231
Sigalotti, L. D. G., de Felice, F., & Sira, E. 2002, A&A, 395, 321
Sigalotti, L. D. G., de Felice, F., & Daza-Montero, J. 2009, ApJ, 707, 1438
Shu, F. H. 1977, ApJ, 214, 488
van der Tak, F. F. S., van Dishoeck, E. F., Evans, N. J., II, & Blake, G. A. 2000, ApJ, 537, 283

S. Lizano: Instituto de Radioastronomía y Astrofísica, UNAM, Apartado Postal 3-72, 58089 Morelia, Michoacán, México (s.lizano@crya.unam.mx).
A. C. Raga and J. C. Rodríguez-Ramírez: Instituto de Ciencias Nucleares, Universidad Nacional Autónoma de México, Ap. 70-543, 04510, Ciudad de México, México (raga, juan.rodriguez@nucleares.unam.mx).